JOURNAL OF SOLID STATE CHEMISTRY 104, 131–148 (1993)

The Reaction between H–Nb_2O_5 (c) and WO_3 (g)

M. W. VICCARY* AND R. J. D. TILLEY†

School of Materials Science, University of Bradford, Bradford, West Yorkshire BD7 1DP, United Kingdom, and †School of Engineering, University of Wales, Cardiff, P.O. Box 917, Newport Road, Cardiff CF2 1XH, United Kingdom

Received October 29, 1992; accepted November 9, 1992

The reaction between crystalline H–Nb_2O_5 and WO_3 vapor was investigated at temperatures between 1200 and 1573 K by means of transmission and scanning electron microscopy, optical microscopy, powder X-ray diffraction, and gravimetric techniques. Below 1254 K the reaction taking place was

$$H\text{–}Nb_2O_5 \rightarrow W_3Nb_{14}O_{44} \rightarrow W_9Nb_8O_{47},$$

while at temperatures above 1254 K the reaction scheme included the phase $6Nb_2O_5 \cdot WO_3$, thus:

$$H\text{–}Nb_2O_5 \rightarrow WNb_{12}O_{33} \rightarrow W_3Nb_{14}O_{44} \rightarrow W_9Nb_8O_{47}.$$

No other phases were formed. The initial reaction of H–Nb_2O_5 is homogeneous and takes place throughout the crystal by way of Wadsley–Andersson diffusion steps to give a product phase mostly consisting of disordered rows of $(5 \times 3)_1$ and $(4 \times 3)_1$ blocks running more or less parallel to the *a*-axis of H–Nb_2O_5. The transformation of this material to $WNb_{12}O_{33}$ and hence to $W_3Nb_{14}O_{44}$ involves similar Wadsley–Andersson shifts which take place in a cooperative fashion to convert one structure to another in a strip by strip fashion. The kinetics of these reactions was recorded. The overall reaction rate followed a simple parabolic rate law despite the complexity of the crystallographic changes taking place.

Introduction

J. S. Anderson recognized at an early stage that high resolution transmission electron microscopy could provide unique insights into the structures of nonstoichiometric compounds and the way in which they reacted. Subsequently he and his co-workers published a number of studies in which the technique of transmission microscopy was exploited, especially with respect to reactions involving the H–Nb_2O_5 "block structures" (see, as examples, *1*, *2*). With respect to these studies he was apt to remark that examining electron micrographs was rather similar to examining evidence in a coroner's court; one had to reconstruct the crime from rather fragmentary data. In this paper electron microscope techniques are employed in a study closely akin to those carried out by J. S. Anderson, that of the reaction of H–Nb_2O_5 crystals with WO_3.

The structure of H–Nb_2O_5 was originally determined by Gatehouse and Wadsley (*3*). The structure is shown in Fig. 1. Early electron microscope studies by Anderson *et al.* (*4*) and Iijima (*5*) revealed that the structure could readily be imaged as an array of blocks

0022-4596/93 $5.00

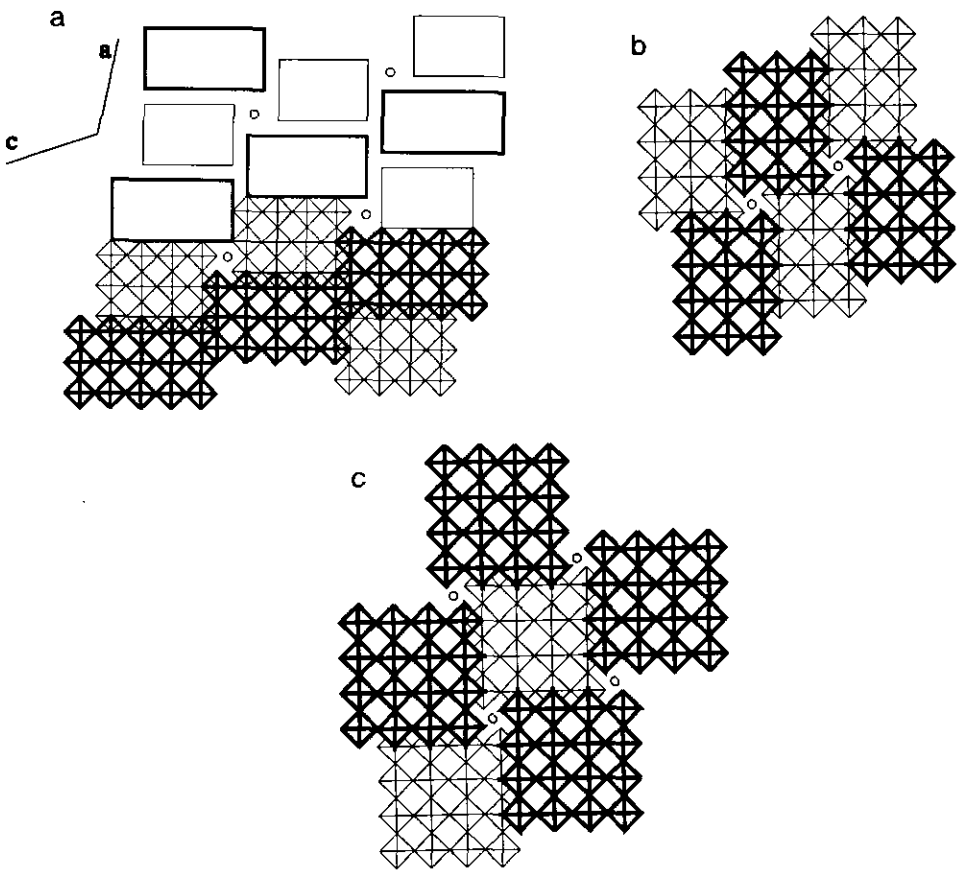

FIG. 1. The idealized structures of (a) H–Nb_2O_5, (b) $WNb_{12}O_{33}$, and (c) $W_3Nb_{14}O_{44}$. The shaded squares represent MO_6 octahedra at two levels in the structure and the circles cations in tetrahedral coordination. In (a) the structure is also represented in a simpler form as packed rectangles and the directions of the crystallographic axes are marked.

and that planar faults in the crystals could be characterized. The equilibrium phase diagram for the H–Nb_2O_5–WO_3 system has been published by Roth and Waring (*6*). The part of the diagram of relevance to the present study is shown in Fig. 2 and the structures of the two other phases central to the reactions occurring, $WNb_{12}O_{33}$ and $W_3Nb_{14}O_{44}$, are also shown in Fig. 1. Besides the known equilibrium phases represented in Fig. 2, a number of other structures, many of which may be metastable, have been described by Gruehn and coworkers (see, e.g., *7–12*).

As part of a series of studies on the reaction of H–Nb_2O_5 and H–Ta_2O_5 with oxide vapors (*13*) we have investigated the reaction between H–Nb_2O_5 and WO_3 vapor. No study of the reaction between solid H–Nb_2O_5 and WO_3 vapor has been reported previously. The object of these studies was to piece together the mechanisms by which the starting material, well crystallized H–Nb_2O_5, transformed into the ternary oxide products of the reaction. The results are presented in this paper as a tribute to the work of J. S. Anderson in this area of endeavour.

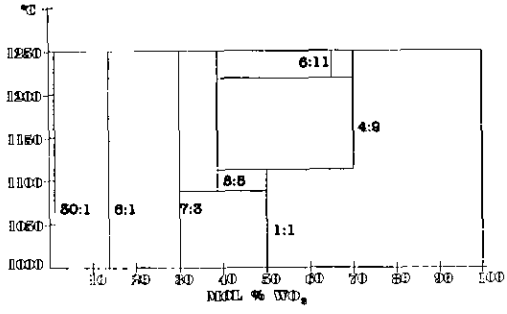

FIG. 2. Part of the equilibrium phase diagram of the H–Nb_2O_5/WO_3 system, redrawn after (6). The figures alongside the phase lines give the molar ratio Nb_2O_5 : WO_3 in the phases. The compound 6 : 1 is $WNb_{12}O_{33}$, 7 : 3 is $W_3Nb_{14}O_{44}$, 1 : 1 is WNb_2O_8, and 4 : 9 is $W_9Nb_8O_{47}$.

Experimental

The phases $WNb_{12}O_{33}$ ($6Nb_2O_5 \cdot WO_3$), $W_3Nb_{14}O_{44}$ ($7Nb_2O_5 \cdot 3WO_3$), and $W_9Nb_8O_{47}$ ($4Nb_2O_5 \cdot 9WO_3$) were prepared from appropriate proportions of Johnson Matthey Specpure grade Nb_2O_5 and WO_3. Each mixture was ground in an agate mortar and pressed in a steel die, placed in a platinum crucible and heated at 973 K for 11 days followed by 1473 K for 4 days, before being air cooled. Products were examined by powder X-ray diffraction and electron microscopy to confirm that they were monophasic.

Before the Specpure H–Nb_2O_5 was used in reactions it was treated in one of four ways, as follows.

SMNb1: annealed in a Pt crucible in air at 1450 K for 3 days and subsequently air cooled.

SMNb2: argon arc melted, annealed in a Pt crucible in air at 1473 K for two days, and subsequently air cooled. Crushed pieces of 0.25–0.5 mm diameter were used.

SMNb3a: argon arc melted, annealed in a Pt crucible in air at 1473 K for five days, and subsequently air cooled. Crushed pieces of 0.25–0.5 mm diameter were used.

SMNb3b: as SMNb3a, but pieces were uncrushed and had an average diameter of 4 mm.

These materials were checked by X-ray powder diffraction and electron microscopy before use.

The starting materials for the reactions were H–Nb_2O_5, $WNb_{12}O_{33}$, or $W_9Nb_8O_{47}$ (prepared as above) and Specpure grade WO_3. Reactions were carried out in a platinum crucible with a sealed platinum lid. The crucible was filled to about $\frac{2}{3}$ capacity with powdered WO_3 and the second reactant, H–Nb_2O_5, $WNb_{12}O_{33}$, or $W_9Nb_8O_{47}$ was placed in a platinum boat on a platinum wire gantry so that it was separated from the WO_3 by an air gap of several mm. The reaction chamber, when primed with reactants, was placed into a furnace which had been preset to the required temperature. The reaction was timed from the moment that the furnace door closed. After the correct time had elapsed the crucible was rapidly removed and allowed to cool in air. Furnace temperatures were controlled and also monitored continuously by way of Pt/Pt–13%Rh thermocouples. Reaction temperatures were considered accurate to ±15 K except for some which were considered to be accurate to ±5 K, as indicated in Table I. For reactions carried out for short heating times the real temperature variation was much smaller than these figures suggest. In some reactions the boat was weighed before and after heating to provide a measure of the overall extent of reaction.

The products of all reactions were examined optically using Zeiss Ultraphot or Olympus stereomicroscopes and via powder X-ray diffraction using a Guinier-Hägg focusing camera employing strictly monochromatic Cu$K\alpha_1$ radiation and KCl (a_0 = 6.29228 Å) as an internal standard. When required, films were measured using a traveling microscope against a scale printed onto the film before development. Selected samples were examined in a Jeol 100B transmission electron microscope fitted with a ±30° double tilt specimen holder operated at 100 kV. For this, samples were crushed

TABLE I

X-RAY DIFFRACTION PHASE ANALYSIS FOR THE REACTION OF H-Nb_2O_5 (c) AND WO_3 (g)

Starting materials[a]	Temperature (K)	Time (hr)	Phase analysis[b]	mol% WO_3[c]
1	1200	16.00	Nb_2O_5	
1	1200	24.00	Nb_2O_5, $W_3Nb_{14}O_{44}$	
1	1200	48.00	Nb_2O_5, $W_3Nb_{14}O_{44}$	
1	1215[d]	20.00	Nb_2O_5, $W_3Nb_{14}O_{44}$	12.7
3a	1220	24.00	Nb_2O_5, ($W_3Nb_{14}O_{44}$)	
3a[e]	1220	72.00	Nb_2O_5, $W_3Nb_{14}O_{44}$	
1	1240	1.00	Nb_2O_5	
1	1240	2.00	Nb_2O_5	
1	1240	3.00	Nb_2O_5, ($W_3Nb_{14}O_{44}$)	
1	1240	4.00	Nb_2O_5, ($W_3Nb_{14}O_{44}$)	
1	1240	5.00	Nb_2O_5, $W_3Nb_{14}O_{44}$	
1[e]	1240	6.00	Nb_2O_5, $W_3Nb_{14}O_{44}$	
1	1240	7.00	Nb_2O_5, $W_3Nb_{14}O_{44}$	
1[e]	1240	8.00	Nb_2O_5, $W_3Nb_{14}O_{44}$	
1[e]	1240	10.00	Nb_2O_5, $W_3Nb_{14}O_{44}$	
1[e]	1240	12.00	Nb_2O_5, $W_3Nb_{14}O_{44}$	
1	1240	14.00	Nb_2O_5, $W_3Nb_{14}O_{44}$	
1[e]	1240	16.00	Nb_2O_5, $W_3Nb_{14}O_{44}$	
1[e]	1240	18.00	$W_3Nb_{14}O_{44}$, Nb_2O_5	
1	1240	20.00	$W_3Nb_{14}O_{44}$, Nb_2O_5	
1	1240[d]	20.00	Nb_2O_5, $W_3Nb_{14}O_{44}$	15.3
1	1240	22.00	$W_3Nb_{14}O_{44}$, (Nb_2O_5)	
1	1240	24.00	$W_3Nb_{14}O_{44}$	
1	1240	48.00	$W_3Nb_{14}O_{44}$, ($W_9Nb_8O_{47}$)	
1	1240	96.00	$W_9Nb_8O_{47}$, $W_3Nb_{14}O_{44}$	
3a[e]	1253	16	Nb_2O_5, $W_3Nb_{14}O_{44}$, ($WNb_{12}O_{33}$)	9.4
1	1255[d]	20.00	Nb_2O_5, $W_3Nb_{14}O_{44}$, $WNb_{12}O_{33}$	14.4
1	1257[d]	20.00	Nb_2O_5, $W_3Nb_{14}O_{44}$, $WNb_{12}O_{33}$	15.1
1	1268[d]	20.00	$W_3Nb_{14}O_{44}$, $WNb_{12}O_{33}$, Nb_2O_5	18.2
2[e]	1273	22	Nb_2O_5, $W_3Nb_{14}O_{44}$ $W_9Nb_8O_{47}$	21.7
1[e]	1373	0.5	Nb_2O_5 (top) Nb_2O_5 (bulk)	1.0
1	1373	1	Nb_2O_5, ($WNb_{12}O_{33}$)	
1	1373	2	Nb_2O_5, $WNb_{12}O_{33}$	
1	1373	3	$WNb_{12}O_{33}$, $W_3Nb_{14}O_{44}$, (Nb_2O_5)	
1[e]	1403	0.25	Nb_2O_5	
1	1423	0.25	Nb_2O_5, ($WNb_{12}O_{33}$)	
1[e]	1423	0.50	Nb_2O_5, $WNb_{12}O_{33}$ (top) Nb_2O_5 (bulk)	2.25
1	1423	1.00	$WNb_{12}O_{33}$, (Nb_2O_5), ($W_3Nb_{14}O_{44}$)	
2	1423	24.00	Nb_2O_5, $WNb_{12}O_{33}$, $W_3Nb_{14}O_{44}$ Nb_2O_5, ($WNb_{12}O_{33}$), ($W_3Nb_{14}O_{44}$)	
2	1423	120	$W_9Nb_8O_{47}$, (Nb_2O_5), ($WNb_{12}O_{33}$) ($W_3Nb_{14}O_{44}$) (top) Nb_2O_5, $W_9Nb_8O_{47}$, ($WNb_{12}O_{33}$) ($W_3Nb_{14}O_{44}$) (bulk)	

TABLE I—*Continued*

Starting materials[a]	Temperature (K)	Time (hr)	Phase analysis[b]	mol% WO_3[c]
1	1423	120	$W_9Nb_8O_{47}$	
1[e]	1473	0.25	Nb_2O_5, $WNb_{12}O_{33}$	
1	1473	0.50	$W_3Nb_{14}O_{44}$	
1[e]	1473	0.50	$W_3Nb_{14}O_{44}$, ($WNb_{12}O_{33}$) (top) $WNb_{12}O_{33}$, Nb_2O_5 (bulk)	16.6
1	1473	1.00	$W_3Nb_{14}O_{44}$, $W_9Nb_8O_{47}$	
1	1473	2.00	$W_3Nb_{14}O_{44}$, $W_9Nb_8O_{47}$	
1	1473	4.00	$W_9Nb_8O_{47}$, $W_3Nb_{14}O_{44}$ (top) $W_3Nb_{14}O_{44}$ (bulk)	84.1
1	1473	4.00	$W_9Nb_8O_{47}$, $W_3Nb_{14}O_{44}$	
1	1473	8.00	$W_9Nb_8O_{47}$, ($W_3Nb_{14}O_{44}$)	
1	1473	16.00	$W_9Nb_8O_{47}$	
1	1473	24.00	$W_9Nb_8O_{47}$	
1	1473	72.00	$W_9Nb_8O_{47}$	
1[e]	1523	0.50	$W_3Nb_{14}O_{44}$, $W_9Nb_8O_{47}$ (top) $W_3Nb_{14}O_{44}$, $WNb_{12}O_{33}$ (bulk)	37.6
1	1523	4.00	$W_9Nb_8O_{47}$	200.3
1	1573	0.50	$W_9Nb_8O_{47}$, $W_3Nb_{14}O_{44}$ (top) $W_3Nb_{14}O_{44}$, $W_9Nb_8O_{47}$ (bulk)	124.2

[a] The starting materials 1, 2, etc. refer to the preparations SMNb1, SMNb2, etc.
[b] The phases are listed in decreasing amounts; those only found in traces are bracketed.
[c] The gain in weight nomalized to H-Nb_2O_5 = 100% at start of reaction.
All temperatures are accurate to ±15 except those marked [d] which are accurate to ±5.
[e] These samples used for electron microscope examination.

in an agate mortar under *n*-butanol and a drop of the resultant suspension allowed to dry on a copper support grid coated with a holey carbon film. Crystal fragments which could be correctly oriented were photographed at a direct magnification of 500,000×.

Results

Phase Analysis

The results of the X-ray phase analysis of the reaction between H-Nb_2O_5 and WO_3 vapor are summarized in Table I. Inspection of these data shows, as expected, that the samples were multiphasic and not at equilibrium. This was also indicated by the fact that the upper part of the reactant H-Nb_2O_5 charge was often lemon yellow while that below the surface remained white, especially in reactions at lower temperatures or shorter heating times. In such cases X-ray diffraction patterns were taken from several regions and two analyses are given in Table I when appropriate, one for material taken from the top of the sample, labeled top, and the other from lower in the sample, labeled bulk.

The powder X-ray diffraction results showed that at temperatures below 1254 ± 9 K the reactions taking place were

$$H\text{-}Nb_2O_5 \rightarrow W_3Nb_{14}O_{44} \rightarrow W_9Nb_8O_{47},$$

while at temperatures of above 1254 ± 9 K the reaction scheme included the phase $6Nb_2O_5 \cdot WO_3$, thus:

$$H\text{-}Nb_2O_5 \rightarrow WNb_{12}O_{33} \rightarrow W_3Nb_{14}O_{44} \rightarrow W_9Nb_8O_{47}.$$

TABLE II

GRAVIMETRIC AND X-RAY ANALYSIS FOR THE REACTION H–Nb_2O_5 (c) AND WO_3 (g)

Reaction time	mol% grav.	WO_3[a] calc.	X-ray phase analysis
10 min			Nb_2O_5, $WNb_{12}O_{33}$, $W_3Nb_{14}O_{44}$, ($W_9Nb_8O_{47}$)
24 hr	4.1	4.1	
48 hr	6.1	6.0	
90 hr	8.5	8.5	
162 hr	11.8	11.8	
258 hr	15.0	15.3	
328 hr	17.6	17.5	
400 hr			$W_9Nb_8O_{47}$ (outer)
			$W_9Nb_8O_{47}$, $WNb_{12}O_{33}$, $W_3Nb_{14}O_{44}$, Nb_2O_5 (inner)

Note. All samples were heated at 1440 ± 20 K. The phases are listed in decreasing amounts; those in traces are bracketed.

[a] grav = gravimetric analysis, calc = calculated from $0.698t^{0.556}$.

Kinetics of Reaction

Gravimetric analysis suggested that the reaction between H–Nb_2O_5 and WO_3 vapor was faster just below 1254 K than slightly above that temperature. In order to verify this a short series of experiments were carried out in which powder samples were heated under carefully controlled conditions for 20 hr in a narrow band of temperatures between 1240 and 1268 K. The results are contained in Table I and are marked by a double asterisk. The crucial results are at 1240 K where 15.3 mol% WO_3 was gained in 20 hr compared with only 14.4 mol% WO_3 at 1255 K, which confirmed the supposition.

In order to obtain information on the rate of the reaction at a constant temperature a series of experiments were carried out in which large pieces of H–Nb_2O_5 were heated to 1440 K for the times shown in Table II and the subsequent weight gains recorded. The rate of reaction is shown in Fig. 3. The curve of weight gain versus time is close to parabolic and was well fitted by the equation

$$\text{weight gain} = 0.698t^{0.556}.$$

Optical Microscopy and Scanning Electron Microscopy

All samples were studied optically after reaction. The overall color of the reaction products was found to change noticeably over the course of about 6 weeks. However, the initial color was regenerated if the samples were heated to about 450 K overnight. X-ray powder photographs of these samples before and after heat treatment showed no changes compared to the original photographs taken immediately after reaction and it is concluded that color changes are due to water absorption on the surface of the powders.

Optical examination revealed the pres-

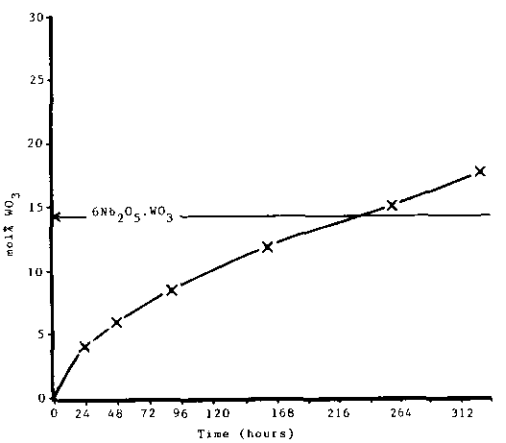

FIG. 3. Gravimetric analysis results for the reaction between H–Nb_2O_5 (c) and WO_3 (g) at 1440 K.

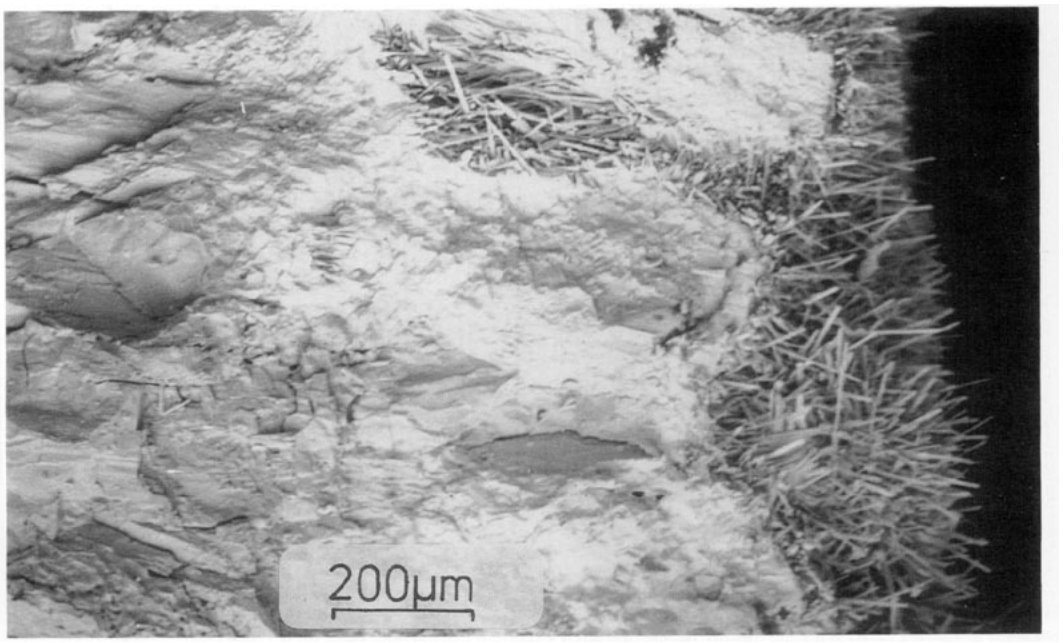

FIG. 4. Scanning electron micrograph of fracture section of H-Nb_2O_5 (SMNb3b) reacted at 1440 K for 400 hr. The needle growth on the surface consists of $W_9Nb_8O_{47}$. No clear distinction is found between the inner H-Nb_2O_5 core and the $WNb_{12}O_{33}/W_3Nb_{14}O_{44}$.

ence of crystals with a fine needle-like habit in samples heated at higher temperatures or for longer periods of time at lower temperatures. These always coincided with the presence of $W_9Nb_8O_{47}$ on X-ray powder patterns and are taken as diagnostic of this phase.

Scanning electron microscopy of the large crystal pieces used for reaction kinetics experiments, detailed above and in Table II, revealed that at quite early stages of reaction the outer part of the material transformed into fine needles which grew to form a thick outer layer. On the other hand, no consistent differences could be found between the morphology of the H-Nb_2O_5 core region and the region containing $WNb_{12}O_{33}$ and $W_3Nb_{14}O_{44}$. Figure 4 shows these microstructures. In order to determine the crystallographic nature of the reaction products the outer surface of a crystal reacted for 10 min was examined by X-ray diffraction, by scraping the surface onto tape using a clean scalpel. A similar procedure was adopted for the crystals reacted for 400 hr, but in this case the outer layer was initially examined and then the material under this layer was also extracted for examination. The results are shown in Table II. It seems reasonable to conclude that the fine needles are $W_9Nb_8O_{47}$, in agreement with the earlier findings, and that the columnar crystals are the block structures $WNb_{12}O_{33}$ and $W_3Nb_{14}O_{44}$.

Transmission Electron Microscopy

Most of the crystal fragments which could be aligned correctly and imaged were found to be well ordered. Of the material reacted at temperatures below 1254 K, 60 out of 74 fragments aligned proved to be of H-Nb_2O_5 which contained no defects other than (101) twin boundaries, which are commonplace in this material (*4*, *5*). Only 2 fragments that appeared to be in the course of reaction

could be imaged. Similarly, of 12 fragments of $W_3Nb_{14}O_{44}$ found, only 2 contained defects that could be imaged and related to the reaction; 4 were well ordered and 6 gave diffraction patterns showing some degree of streaking.

A similar picture emerged from the material which was heated to temperatures above 1254 K. Of 87 fragments of H–Nb_2O_5 examined, 69 contained no defects or (101) twins, 9 yielded difraction patterns with some form of streaking, and only 9 showed any discernable block disorder. In the case of $WNb_{12}O_{33}$ 15 fragments were perfect, 2 gave diffraction patterns with some degree of streaking, and 5 showed any block disorder. For $W_3Nb_{14}O_{44}$ 11 fragments were perfect, 1 gave a diffraction pattern with some streaking, and only 3 showed any block disorder. All fragments of $W_9Nb_8O_{47}$ observed were defect free.

Despite this paucity of reaction data a relatively consistent picture emerges of the reaction process. The initial stage of reaction is typified by the crystal fragment shown in Fig. 5 which was recovered from the products of reaction at 1240 K for 8 hr. This had a diffraction pattern of the H–Nb_2O_5 type despite the considerable disorder visible in Fig. 5. The first stage of the transformation was penetration of the H–Nb_2O_5 by WO_3 species down the *b*-direction along the block edges, indicated by dark regions of ill defined contrast which occur at the block edges. From the micrographs examined it was clear that the reaction was proceeding at many different points in the crystal. The originally parallel and ordered array of blocks in the starting material has become disordered and the crystal becomes a mosaic of domains of slightly differing block types. The block edges become wavy, especially in a direction along the short block edges, which is roughly parallel to the original H–Nb_2O_5 *a*-axis. These effects are due to the transformation of the original matrix into parallel disordered rows of predominately $(5 \times 3)_1$ and $(4 \times 3)_1$ blocks. The meandering nature of the boundaries is due to different proportions of the two block types present and to the fact that rows of $(5 \times 3)_1$ and $(4 \times 3)_1$ blocks cannot be formed exactly parallel to the *a*-axis of the parent structure (*vide infra*). Distinct domains of $(5 \times 3)_2$ and $(4 \times 3)_1$ structure are also present. This latter structure is that of $WNb_{12}O_{33}$, even though this phase does not form in macroscopic amounts at the temperature of the reaction which produced the crystal in Fig. 5.

Slightly later stages of reaction are documented in Figs. 6 and 7. Fig. 6 shows a crystal which gave a $WNb_{12}O_{33}$ type of diffraction pattern, obtained from a sample heated to 1253 K for 16 hr. Much of the matrix consists of disordered parallel rows of $(5 \times 3)_1$ and $(4 \times 3)_1$ blocks. A variety of other block types including domains of $(4 \times 3)_1$ blocks and a domain of $(5 \times 3)_2$ blocks can also be identified. Reaction along the short block edges is revealed by dark contrast at these junctions. Fig. 7 shows a crystal heated to 1423 K for $\frac{1}{4}$ hr in which the twinned structure of H–Nb_2O_5 is still apparent in some regions. The predominant microstructure again consists of disordered parallel strips of $(4 \times 3)_1$ and $(5 \times 3)_1$ structure, although domains of different block sizes are not uncommon. The impression given is that the reaction is much more orderly at this higher temperature and that the formation of the $(4 \times 3)_1$ and $(5 \times 3)_1$ structure is now virtually complete. Areas of only $(5 \times 3)_1$ blocks can also be distinguished and dark ribbons of contrast along the short block edges suggest that these rows of blocks are in the act of transforming along these sites.

No significant differences could be found between initial reactions above and below 1254 K. Unfortunately the course of the reaction from the initial stage to $W_3Nb_{14}O_{44}$ at temperatures below 1254 K has not been

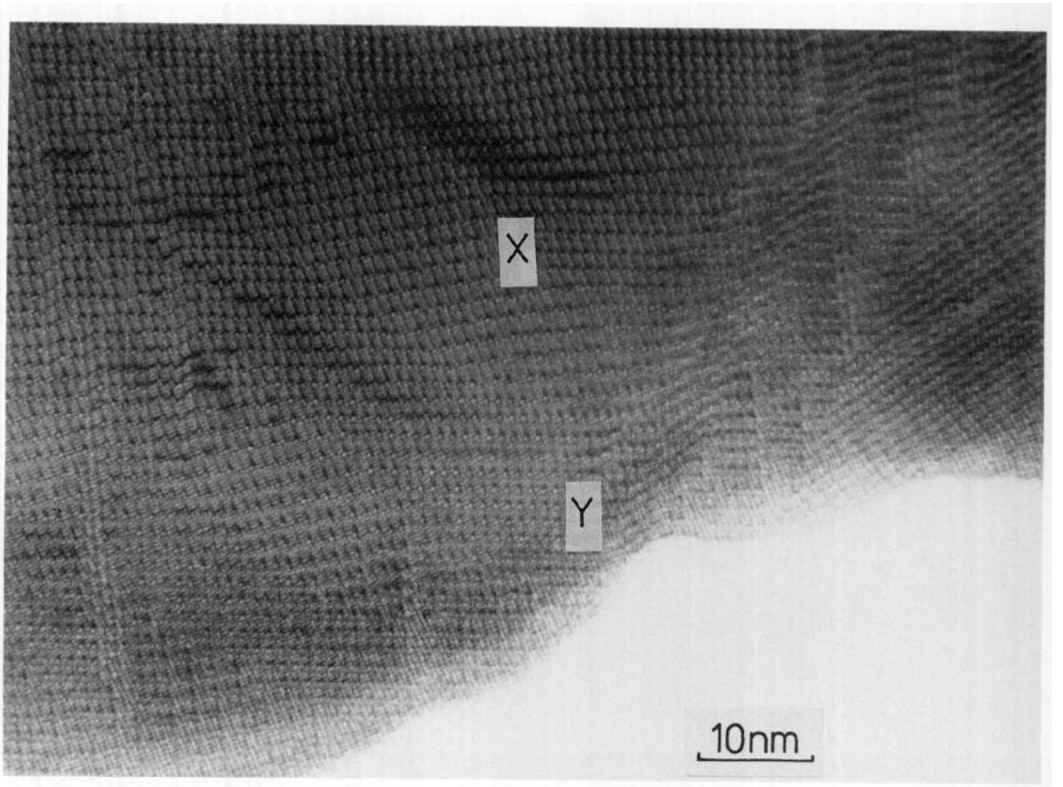

FIG. 5. Electron micrographs of a partly reacted crystal recovered from a reaction at 1240 K for 8 hr. Regions of $(5 \times 3)_2$ structure, marked *X*, and of $(4 \times 3)_1$ structure, marked *Y*, are present. Much of the meandering of the block edges is due to conversion of the original material into intergrown rows of $(5 \times 3)_1$ and $(4 \times 3)_1$ type running roughly parallel to the original H–Nb_2O_5 *a*-axis.

directly revealed on any of the micrographs. More information is available concerning the transformation to $WNb_{12}O_{33}$ and $W_3Nb_{14}O_{44}$ above 1254 K. Figure 8, from a sample heated for $\frac{1}{4}$ hr at 1423 K, shows a crystal consisting of mostly $(4 \times 3)_1$ rows of blocks, but a fair number of parallel disordered $(5 \times 3)_1$ rows are also present. The stage of reaction seems slightly later than in Fig. 7. The $(5 \times 3)_1$ rows have kinks on them suggesting that they are in the course of forming $(4 \times 3)_1$ rows by way of a cooperative mechanism operating along the short block edges. Rather more obvious, though, are sheets of faults consisting of $(4 \times 4)_1$ and blocks intergrown perpendicular to the parallel rows of $(4 \times 3)_1$ and $(5 \times 3)_1$ blocks of the matrix. The appearance of these crystals is strongly suggestive of a situation where the $(4 \times 3)_1$ and $(5 \times 3)_1$ mixture was transforming in a step by step fashion to a $(4 \times 3)_1$ array by converting each existing row of $(5 \times 3)_1$ structure into a $(4 \times 3)_1$ row separately. A second transformation, taking place simultaneously in a direction perpendicular to the first, was already converting the crystal into a $(4 \times 4)_1$ array with random strips reacting at any time.

In all of the micrographs examined no trace of reaction within a block was found as opposed to reaction at block edges.

No information was obtained on the transformation of the block structures to $W_9Nb_8O_{47}$.

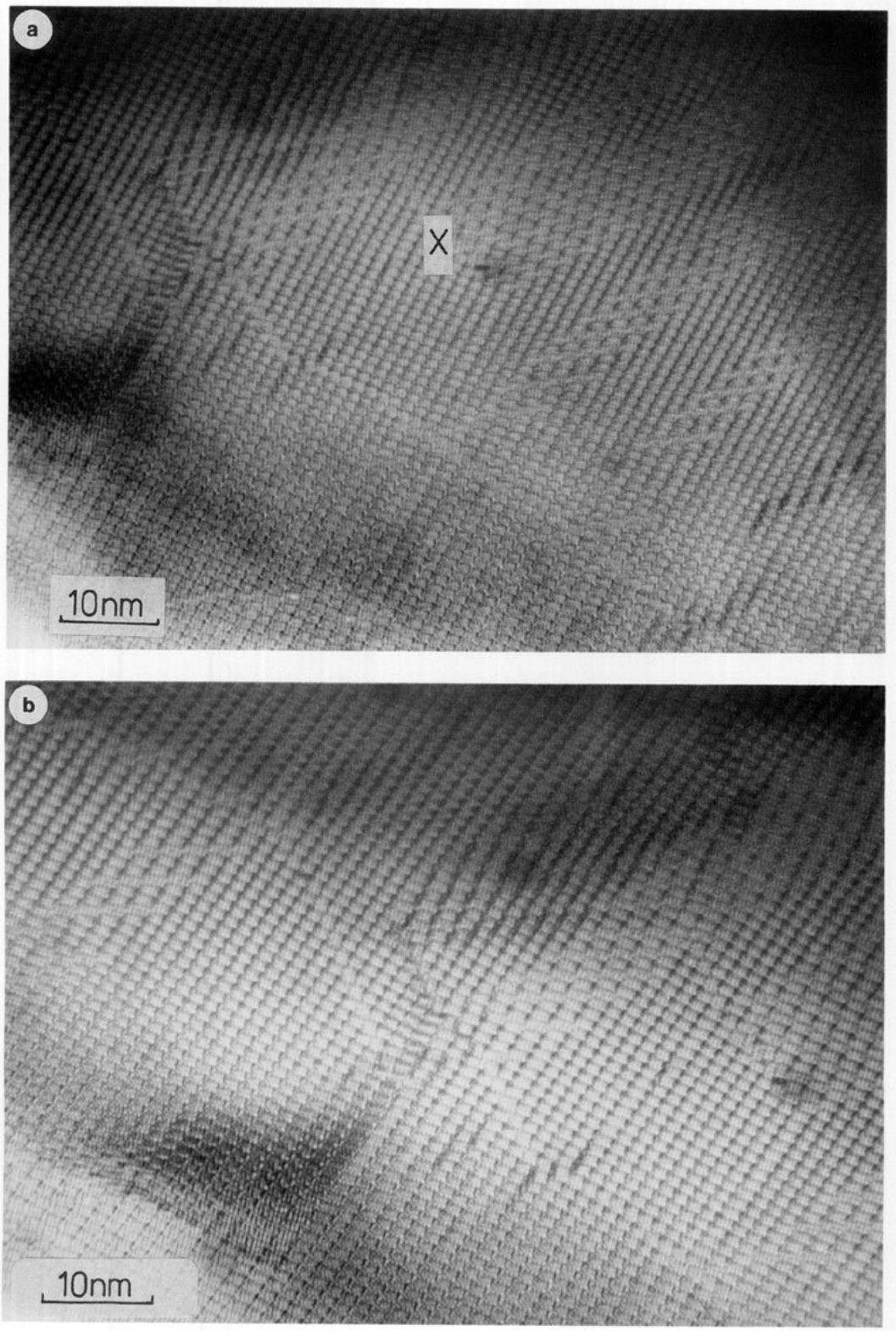
a
X
10nm
b
10nm

The Reaction between $WNb_{12}O_{33}$ or $W_9Nb_8O_{47}$ and WO_3 Vapor

The reaction between $WNb_{12}O_{33}$ and WO_3 vapor was carried out to compare the rate of reaction of $WNb_{12}O_{33}$ with that of H–Nb_2O_5. The results are given in Table III. The powder X-ray diffraction results indicate that the reaction taking place is

$$WNb_{12}O_{33} \rightarrow W_3Nb_{14}O_{44} \rightarrow W_9Nb_8O_{47},$$

although at the lowest temperatures none of the final phase, $W_9Nb_8O_{47}$, was produced, even after 96 hr reaction. In general a comparison of the data in Table I with that in Table III suggested that the reaction between H–Nb_2O_5 and WO_3 was much faster than that between $WNb_{12}O_{33}$ and WO_3. In order to confirm this, quantities of both H–Nb_2O_5 and $WNb_{12}O_{33}$ were placed on separate trays in the same reaction vessel and heated at 1243 K for 20 hr. This temperature was chosen so that the reaction product would be the same in each case, viz., $W_3Nb_{14}O_{44}$, a result confirmed by powder X-ray diffraction. The H–Nb_2O_5 sample gained 13.2 mol% WO_3 while the $WNb_{12}O_{33}$ gained only 5.5 mol% WO_3. A clear difference in reaction rates was shown.

The rate of reaction of $W_9Nb_8O_{47}$ with WO_3 was extremely slow. After 428 hr at 1440 K the sample only gained 4.6 mol% WO_3. The X-ray powder diffraction patterns slowly evolved towards that associated with the $2Nb_2O_5 : 7WO_3$ phase described by Roth and Waring (*6*). It is likely that the real structure of the material is a disordered tetragonal tungsten bronze type of phase (*14*). The disordering process is much slower than the rate of reaction of the block structures.

Discussion

Mechanisms of Block Structure Reactions

The electron microscope evidence showed that the initial reaction proceeded down the *b*-axis and that lines of reaction ran along the short block edges parallel to the *a*-axis of H–Nb_2O_5. The initial well ordered crystals became unscrambled, at a rate depending upon reaction temperature, into a mosaic consisting of more or less disordered strips of $(5 \times 3)_1$ and $(4 \times 3)_1$ material lying roughly parallel to the *a*-axis of H–Nb_2O_5. Despite the X-ray findings, no significant differences in microstructures were found for crystals reacted above 1254 K and below this temperature.

The complex mosiac structure of the crystal fragments examined shows that the initial reaction is homogeneous. The appearance of the crystals at this stage of the reaction was very similar to those observed by Crawford and Anderson (*2*) in their investigations of the oxidation of the lower oxides of niobium to H–Nb_2O_5, apart from the overall difference in block sizes present. This was also a homogeneous reaction and it is reasonable to assume that a similar mechanism operates in both cases. Crawford and Anderson showed that the diffusion mechanism devised by Wadsley and Andersson (*15–17*), which only involves small diffusion steps within the *CS* planes bounding the blocks (an AW shift), could account for all of the transformations that they observed. This diffusion step is shown by the arrows in Fig. 9a. Such AW shifts can readily produce the type of mosiac crystal observed in our experiments and we will assume that this mechanism was responsible for the structures illustrated.

FIG. 6. (a, b) Electron micrographs of a partly reacted crystal recovered from a reaction at 1253 K for 16 hr. The bulk of the structure consists of parallel disordered rows of $(5 \times 3)_1$ and $(4 \times 3)_1$ type running roughly parallel to the original H–Nb_2O_5 *a*-axis. An extensive domain of $(5 \times 3)_2$ structure is seen at X in (a).

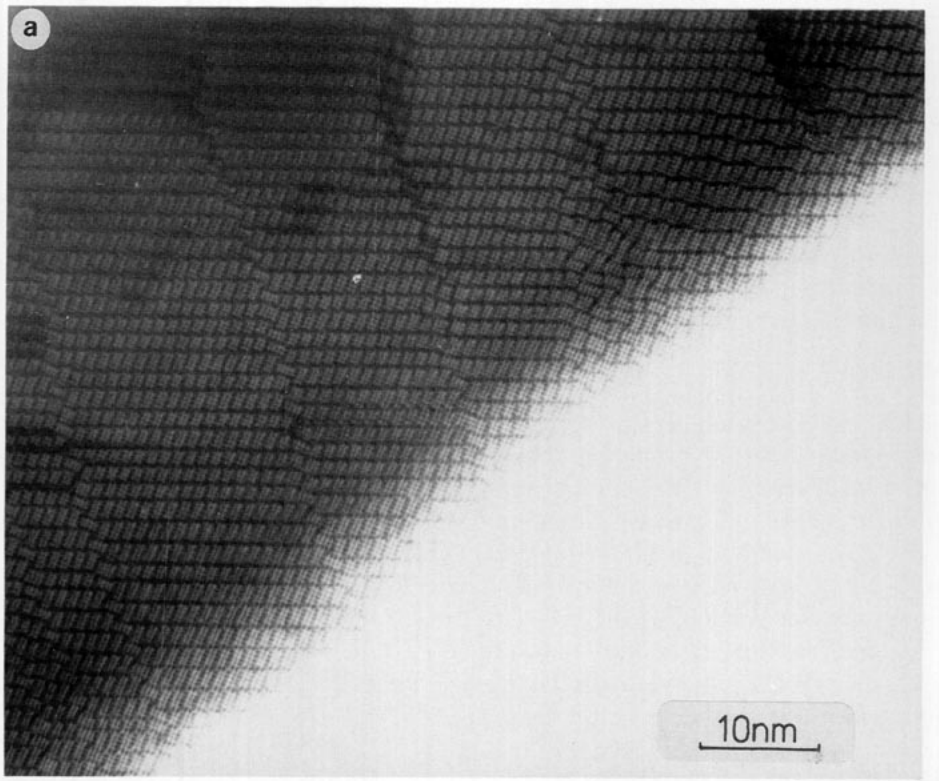
a
10nm

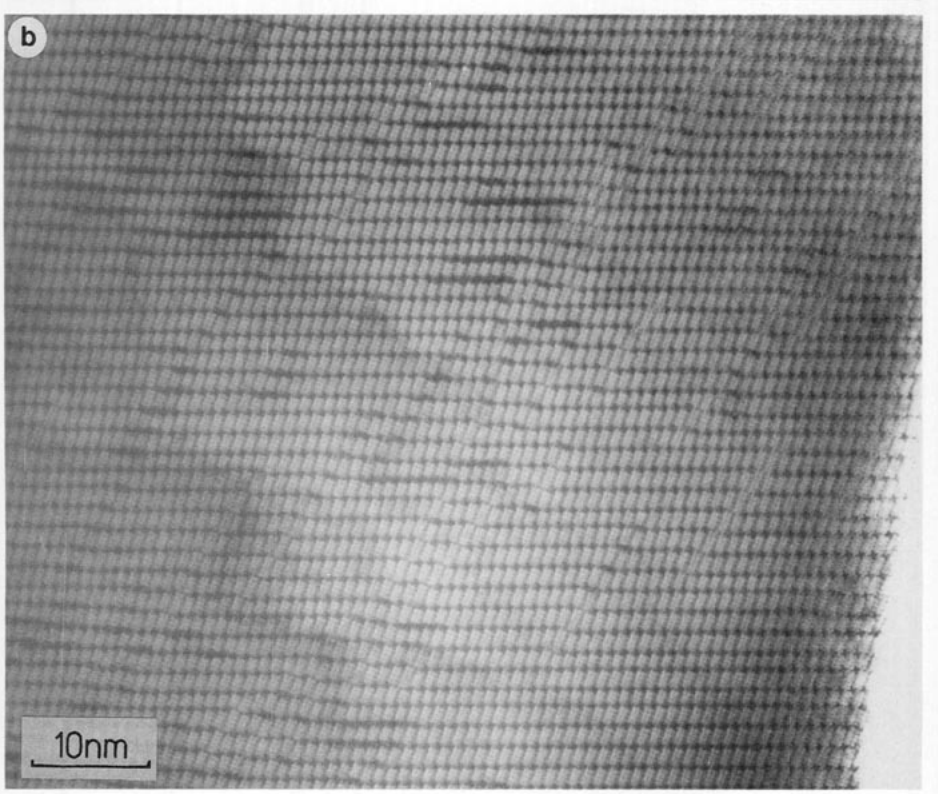
b
10nm

In the present reaction it appears that an important first step is that of "block swapping" which is a term coined by Crawford and Anderson (*2*). Here neighboring $(5 \times 3)_\infty$ and $(4 \times 3)_1$ blocks swap places as part of the process of generating parallel rows of $(5 \times 3)_1$ and $(4 \times 3)_1$ blocks. The AW shift mechanism for part of this reaction, the generation of parallel blocks of $(5 \times 3)_2$ and $(4 \times 3)_2$ is shown in Fig. 9a and b. The first reaction is seen to have taken place exclusively along the short block edges in the crystals.

Although the block swapping reaction seems to be the principal one taking place, the final geometry of this mosaic crystal will reflect several factors. Increase in WO_3 content within any particular volume of crystal will drive the block sizes upward toward $(\infty \times \infty)$ and may account for the large areas of $(5 \times 3)_1$ blocks observed. The geometry of the block structures shows that it is not possible to intergrow $(5 \times 3)_1$ and $(4 \times 3)_1$ rows within the H–Nb_2O_5 structure exactly parallel to the *a*-axis because there is a considerable angle between the *a*-axis and the new row directions. Intergrowth parallel to the *c*-axis is possible and both situations are shown in Fig. 10. Any diffusion mechanism which converts a small region of H–Nb_2O_5 structure into $(5 \times 3)_1$ and $(4 \times 3)_1$ rows soon runs into difficulty because of this angular misfit which contributes to the meandering nature of the boundaries. A final constraint is the necessity to fit all the blocks together in a coherent whole. A combination of these factors then produces the final and complex mosaic microstructure observed at this stage of reaction.

A mechanism for the transformation of H–Nb_2O_5 into the ordered $(4 \times 3)_1$ structure of $MoNb_{12}O_{33}$, a phase isostructural with $WNb_{12}O_{33}$, was proposed by Andersson in 1969 (*16*). This involved cooperative AW shifts and introduced coherently intergrown slabs of $(4 \times 3)_1$ structure parallel to the *c*-axis of H–Nb_2O_5, i.e., on (100) planes. In the present experiments the $(5 \times 3)_1$ and $(4 \times 3)_1$ strips are more or less parallel to the *a*-axis, i.e., on (001) planes. It is thus certain that Andersson's mechanism does not operate in the reactions studied here.

The transformation of the disordered $(5 \times 3)_1$ and $(4 \times 3)_1$ structure into the product $W_3Nb_{14}O_{44}$ at lower temperatures or $WNb_{12}O_{33}$ and then $W_3Nb_{14}O_{44}$ at higher temperatures is the second stage of the reaction. Unfortunately no crystal fragments which directly gave evidence for the low temperature transformation were found. However, the transformation to $WNb_{12}O_{33}$ imaged on crystal fragments shown in Fig. 7b and Fig. 8 shows that this took place by a series of cooperative AW shifts along a direction parallel to the short block edges. The reaction seems to be initiated along random strips in the structure so that a disordered intergrowth represents the intermediate structure observed. In this reaction the overall dimensions of the crystal in the plane of projection imaged is getting smaller. This suggests that the diffusion step is taking material from the short edges of the $(5 \times 3)_1$ blocks to the surface of the crystal where it is able to react with more WO_3 to form a surface layer of the $(4 \times 3)_1$ phase or else $W_9Nb_8O_{47}$ needles.

The third stage of the reaction, to form $W_3Nb_{14}O_{44}$, is captured in Fig. 8. Once again a cooperative AW shift mechanism oper-

FIG. 7. (a, b) Electron micrographs of two regions of a crystal recovered from a reaction at 1423 K for $\frac{1}{2}$ hr. The bulk of the structure consists of disordered rows of $(5 \times 3)_1$ and $(4 \times 3)_1$ type running roughly parallel to the original H–Nb_2O_5 *a*-axis. Remnant twins which occurred in the original crystal are visible in (a) and dark strips of contrast running along block edges where ribbons of $(5 \times 3)_1$ blocks appear to be changing to ribbons of $(4 \times 3)_1$ blocks are visible in both photographs.

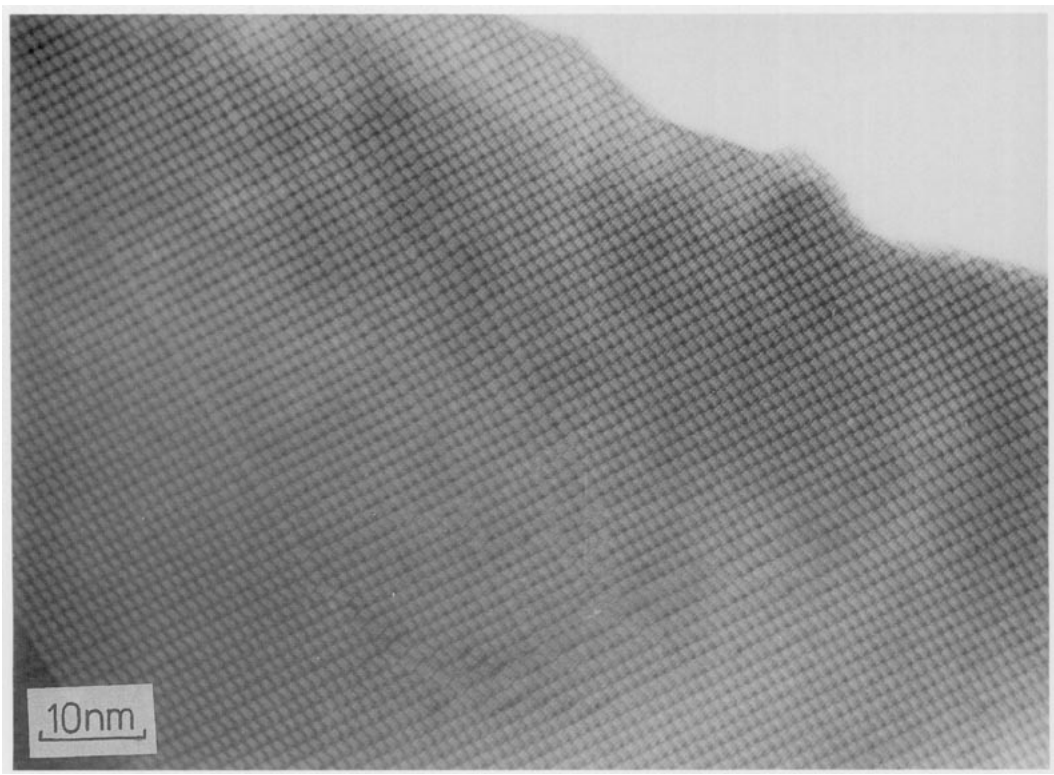

FIG. 8. Electron micrograph of a partly reacted crystal which was mainly $WNb_{12}O_{33}$. The structure still contains disordered rows of $(5 \times 3)_1$ intergrown with the $(4 \times 3)_1$ type and also strips of intergrown $(4 \times 4)_1$ structure running perpendicular to these rows. Other block sizes are also present.

TABLE III

X-RAY PHASE ANALYSIS FOR THE REACTION OF $WNb_{12}O_{33}$ (c) AND WO_3 (g)

Reaction temperature (K)	Reaction time (hr)	mol% WO_3 gained	X-ray phase analysis
1243	2	0.3	$WNb_{12}O_{33}$
1243	16	1.8	$WNb_{12}O_{33}$, $(W_3Nb_{14}O_{44})$
1243	20	2.8	$WNb_{12}O_{33}$, $(W_3Nb_{14}O_{44})$
1243	24	4.7	$WNb_{12}O_{33}$, $(W_3Nb_{14}O_{44})$
1243	48	7.9	$WNb_{12}O_{33}$, $W_3Nb_{14}O_{44}$
1243	96	14.0	$W_3Nb_{14}O_{44}$, $WNb_{12}O_{33}$
1273	20	5.4	$WNb_{12}O_{33}$, $W_3Nb_{14}O_{44}$
1473	2.25		$W_3Nb_{14}O_{44}$
1473	4.5		$W_3Nb_{14}O_{44}$, $W_9Nb_8O_{47}$
1473	18		$W_9Nb_8O_{47}$, $(W_3Nb_{14}O_{44})$

Note. The phases are listed in decreasing amounts; those only found in traces are in parentheses.

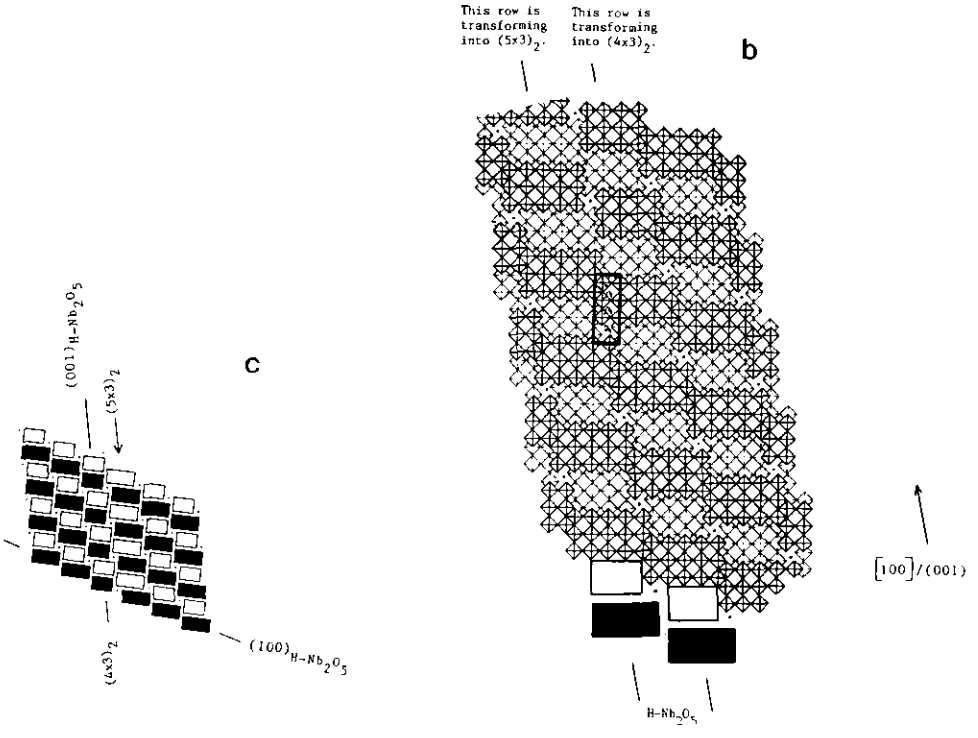

FIG. 9. The transformation of the $(5 \times 3)_x + (4 \times 3)_1$ structure of H–Nb_2O_5 into a structure containing $(5 \times 3)_2$ and $(4 \times 3)_2$ rows. (a) shows the atomic diffusion steps required, which are represented by curved arrows. These diffusion steps constitute an AW shift which move a block edge by one octahedron. (b) shows the result of the steps in (a). The area undergoing the AW shift is enclosed in a box. The product structure, (c), contains a pair of $(5 \times 3)_2 + (4 \times 3)_2$ rows which lie parallel to the original *a*-axis of H–Nb_2O_5.

ates. In this, strips of structure, at random, transform along block edges in a direction perpendicular to that in the first two stages. The reaction can be duplicated by the same mechanism that Andersson proposed with respect to $Mo_3Nb_{14}O_{44}$ (*16*) and will not be repeated here.

Crystallographic Aspects

The series of structures which formed were different than those expected from the equilibrium phase diagram. Apart from the small number of block structures found, the pentagonal column phase WNb_2O_8 was not detected in reactions below 1115°C, the temperature above which it disproportionates, and the phase $W_9Nb_8O_{47}$ was detected in many reactions well below the reported minimum stability temperature of the compound, 1150°C. The products of reaction were, in the main, far from equilbrium and the results are a snapshot of the dynamical situation holding in the system. It would therefore be expected that the reactions would be dominated by ones which were fastest and topologically most facile.

The initial reaction of the H–Nb_2O_5 seems to be the same both above and below 1254 K (vide infra) and it has not proved possible to discover why in one case the phase

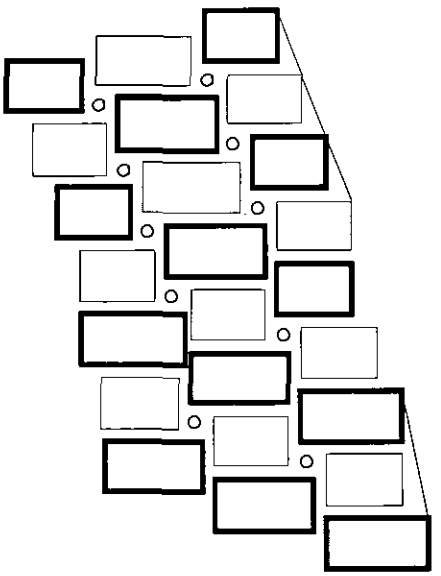

FIG. 10. The structure of the intergrowth between H–Nb_2O_5, lower half of figure, and $(5 \times 3)_1$ and $(4 \times 3)_1$ rows, upper half of figure. The intergrowth is coherent along H–Nb_2O_5 (100) planes but forms an angle with the (001) planes. The lines linking the block edges are a guide for the eye.

$W_3Nb_{14}O_{44}$ is formed directly from H–Nb_2O_5 and in the other $WNb_{12}O_{33}$ forms as an intermediate. The phase diagram of Roth and Waring (*6*) does not cover the lower temperature range used in these studies and when Andersson (*16*) found a similar phenomonon in the reaction of MoO_3 with H–Nb_2O_5 he concluded that stability of the products was responsible. This will be checked for the present case and the results reported.

The results show that the transformation of H–Nb_2O_5 into other block structures is a topotactic reaction. The mechanisms described in the preceding section show why this is so and needs no further comment. The nonoccurrence of the large number of intergrowth phases which have been found in the composition range between H–Nb_2O_5 and $WNb_{12}O_{33}$ can also be understood in terms of the reaction mechanism uncovered. From a structural point of view these intergrowth phases consist of increasing numbers of slabs of the $(4 \times 3)_1$ type coherently intergrown in the parent H–Nb_2O_5 structure on (100) planes, i.e., along the long block edges (*18*). The mechanism of reaction described above shows that the transformations took place more or less parallel to the *a*-axis of H–Nb_2O_5, along the short block edges. It is likely that the nonappearance of other block structures can be attributed to similar mechanistic processes.

The formation of $W_9Nb_8O_{47}$ was quite different. The phase grew from the surface of $W_3Nb_{14}O_{44}$ in the form of very fine needles. The two principal points of interest are why

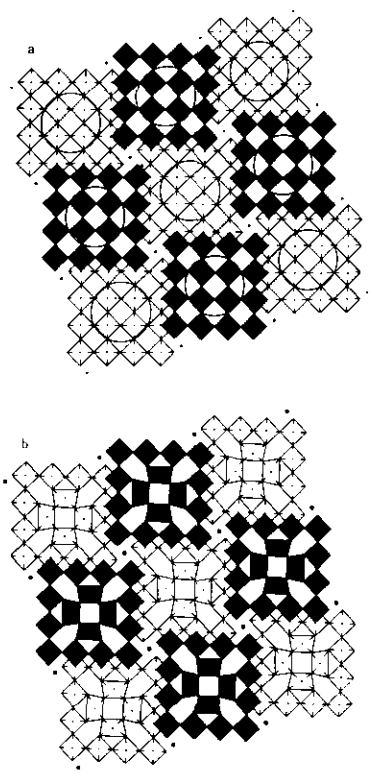

FIG. 11. Rotation of the groups of octahedra circled in (a). The $W_3Nb_{14}O_{44}$ structure leads to a disposition of pentagonal tunnels, (b), identical to that found in the tetragonal tungsten bronze framework of $W_9Nb_8O_{47}$.

the phase $TaWO_8$ was absent and why the formation of the tetragonal tungsten bronze structure $W_9Nb_8O_{47}$ was favored at temperatures well below that reported for its stability limit. Although the mechanism of this transformation was not characterized by electron microscopy it is possible to speculate that the answer to both of these questions may simply be an economy of structural rearrangement. Hyde and O'Keeffe (*19*) put forward an elegant rotation mechanism for the transformation of the ReO_3 structure into the tetragonal tungsten bronze structure. In the present case simply placing a rotation center at the center of each block in the $W_3Nb_{14}O_{44}$ structure, as shown in Fig. 11, generates the skeleton of the tetragonal tungsten bronze structure of $W_9Nb_8O_{47}$ with no errors. The $W_3Nb_{14}O_{44}$ therefore is able to act as a template for the growth of $W_9Nb_8O_{47}$ outward from the surface of these crystals. The same is not true if one tries to generate the WNb_2O_8 structure, as in this case the rotation centers must frequently be positioned over the *CS* planes defining the block walls in $W_3Nb_{14}O_{44}$. The same is true for the other block structures to be found in this system and it is only $W_3Nb_{14}O_{44}$ which allows the formation of $W_9Nb_8O_{47}$ to occur in such a fashion. It is thus tempting to assume that this structural facility controls the course of the reaction.

Kinetic Aspects of the Reaction

The experimental arrangement chosen constrained the reaction to be of the type

$$\text{H–Nb}_2\text{O}_5\ (c) + n\text{WO}_3\ (g) \rightarrow \text{Nb}_2\text{O}_5 : n\text{WO}_3\ (c).$$

The principal molecular species found in the vapor over WO_3 are $(WO_3)_3$ (g), $(WO_3)_4$ (g), and $(WO_3)_5$ (g) (*20–24*). These molecules are composed of tetrahedral WO_4 units, 3, 4, or 5 units long linked in puckered rings. The vapor pressure over solid WO_3 is given by the equation

$$\log_{10}p = 24{,}600/T + 15.63$$

for the temperature range 1000–1708 K, where the pressure, p, is in mm Hg (1 mm Hg = 133.322 Nm^{-2}) and T is the temperature in K (*25*). The rate at which the molecular species collide with the surface, Z, derived from the kinetic theory of gases, has been given by Somorjai (*26*). For the specific case of WO_3, taking into account the relative abundances of the various molecular species present (*21, 24*), it is found that

$$Z = (3.057 \times 10^{21})p/\sqrt{T},$$

where Z is the number of molecules colliding with the surface per m^2, p is the vapor pressure, Nm^{-2}, and T is the temperature in K. This is a smooth parabolic function with no significant discontinuity of either vapor pressure or of rate of arrival of molecular species at a temperature of 1254 K to account for the differences in reaction rate found in the vincinity of this temperature, which must therefore be attributed to crystallographic differences.

The kinetic experiments showed that H–Nb_2O_5 reacted more rapidly just below 1254 K than just above this temperature. As H–Nb_2O_5 is the stable structural form of Nb_2O_5 at all the temperatures investigated the differences found cannot be attributed to structural changes in this reactant. Additionally, H–Nb_2O_5 reacted faster than $WNb_{12}O_{33}$ at 1243 K. This latter result partly explains the first as above 1254 K $WNb_{12}O_{33}$ is the product of the reaction and this must inhibit the rate of reaction compared to $W_3Nb_{14}O_{44}$.

The difference between H–Nb_2O_5 and $WNb_{12}O_{33}$ must be due to the structural differences between the two phases. The $WNb_{12}O_{33}$ structure consists only of $(4 \times 3)_l$ blocks whereas in H–Nb_2O_5 the structure contains both $(5 \times 3)_\infty$ and $(4 \times 3)_l$ blocks. The difference therefore must reside in the $(5 \times 3)_\infty$ blocks. As the electron microscope results show that the reactive sites are the *CS* planes in the block edges it seems rea-

sonable to regard the reactive site in H–Nb_2O_5 as the junctions where the (5 × 3) blocks are joined. These contain metal–oxygen octahedra joined by two edges and can be regarded as the most reduced part of the structure in terms of the local metal to oxygen ratio.

We finally draw attention to the kinetic results presented in Fig. 3. This data showed that the rate of the reaction could be considered as a smooth almost parabolic curve. Such data have often been taken as indicative of a rather simple interdiffusion mechanism of reaction and "activation energies" correspondingly derived. Structural analysis, however, shows that the reactions taking place are complex and that such an interpretation would be far too simplistic in the present case.

Conclusions

The use of transmission electron microscopy in the study of the reactions of block structures, pioneered by J. S. Anderson, has thrown considerable light on the reactivity of the solid substrate at an atomic level of discrimination. The initial transformation is homogeneous and occurs throughout the H–Nb_2O_5 crystals by way of AW shifts at the short block edges in the structure. The major constraint is to accommodate the incoming flux of WO_3 species with a coherent block mosaic. Ensuing transformations of this mosaic takes place by cooperative AW shifts along specific block edges, first the short edge, to generate $WNb_{12}O_{33}$, and then the long edge, to generate $W_3Nb_{14}O_{44}$. A study of reaction kinetics does not reveal the complexity of the crystallographic changes taking place in this solid–vapor reaction. Not all of the details of the reaction have been uncovered and further work still needs to be carried out before all aspects are understood.

Acknowledgments

MWV thanks the Science and Engineering Research Council for the provision of a studentship and RJDT for an equipment grant which allowed this work to be undertaken.

References

1. J. S. Anderson, *Chem. Scr.* **14,** 660 (1978/9).
2. E. S. Crawford and J. S. Anderson, *Philos. Trans. R. Soc. London A* **304,** 327 (1982).
3. B. M. Gatehouse and A. D. Wadsley, *Acta Crystallogr.* **17,** 969 (1966).
4. J. S. Anderson, J. M. Browne, and J. L. Hutchison, *J. Solid State Chem.* **5,** 419 (1972).
5. S. Iijima, *Acta Crystallogr. Sect.A* **29,** 18 (1973).
6. R. S. Roth and J. L. Waring, *J. Res. Natl. Bur. Stand. Sect. A* **70,** 281 (1966).
7. R. Gruehn, *Comm. Inorg. Chem.* **1,** 361 (1982).
8. G. Heurung and R. Gruehn, *J. Less-Common Met.* **76,** 17 (1980).
9. G. Heurung, R. Gruehn, and H. Brunner, *Z. Naturforsch. Sec. B* **34,** 553 (1979).
10. R. Gruehn, *in* "Studies in Solid State Chemistry" (R. Metselaar, H. J. M. Heijligers, and J. Schoonman, Eds.), Vol. 3, p. 33 (1982).
11. H. Groh and R. Gruehn, *Z. Anorg. Allg. Chem.* **503,** 165 (1983).
12. H. Groh, B. Meyer, and R. Gruehn, *Z. Anorg. Allg. Chem.* **497,** 56 (1983).
13. P. J. England and R. J. D. Tilley, *Chem. Scr.* **24,** 130 (1984).
14. P. J. England and R. J. D. Tilley, *Chem. Scr.* **23,** 15 (1984).
15. S. Andersson and A. D. Wadsley, *Nature* **211,** 581 (1966).
16. S. Andersson, *Z. Anorg. Allg. Chem.* **366,** 96 (1969).
17. A. D. Wadsley and S. Andersson, *in* "Perspectives in Structural Chemistry III" (J. D. Dunitz and J. A. Ibers, Eds.), Chap. 1, p. 1, Wiley, New York (1970).
18. J. G. Allpress and A. D. Wadsley, *J. Solid State Chem.* **1,** 28 (1969).
19. B. G. Hyde and M. O'Keeffe, *Acta Crystallogr. Sect. A* **29,** 243 (1973).
20. J. Berkowitz, M. G. Inghram, and W. A. Chupka, *J. Chem. Phys.* **26,** 842 (1957).
21. J. Berkowitz, W. A. Chupka, and M. G. Inghram, *J. Chem. Phys.* **27,** 85 (1957).
22. G. Demaria, R. P. Burns, J. Drowart, and M. G. Inghram, *J. Chem. Phys.* **32,** 1373 (1960).
23. R. J. Ackermann and E. G. Rauh, *J. Phys. Chem.* **67,** 2596 (1963).
24. A. A. Ivanov, A. V. Demidof, N. I. Popenko, E. Z. Zasorin, V. P. Spiridonov, and I. Hargittai, *J. Mol. Struct.* **63,** 121 (1980).
25. O. Kubaschewski and C. B. Alcock, "Metallurgical Thermochemistry," 5th ed. Pergamon, Oxford (1979).
26. G. A. Somorjai, "Principles of Surface Chemistry," Prentice–Hall, New York (1972).